RSC Advances

PAPER

View Article Online
View Journal | View Issue

Cite this: *RSC Adv.*, 2017, **7**, 41909

Heavy metal detoxification by recombinant ferritin from *Apostichopus japonicus*

Kaixue Si,[a] Tinghong Ming,[a] Yanyan Li,[b] Xiaoting Qiu,[a] Liping Chen,[a] Jun Zhou,[a] Chenyang Lu,*[a] Xiurong Su,*[a] Ye Li[a] and Ling-Zhi Cheong[a]

Ferritin is a bionanomaterial that is widely applied in magnetic resonance imaging, drug delivery systems, biocompatible fluorescence, neutron-capture therapy and electrochemical markers. Ferritin also has great potential for use in environmental detection and heavy metal removal due to its hollow cage sequestration and maintenance of iron in a nontoxic and bio-available form. In this study, the heavy metal binding activity of ferritin from *Apostichopus japonicus* (AjFER) was elucidated using scanning electron microscopy (SEM). It was observed that ferritin aggregation morphology changed dramatically upon exposure to five metals. The reaction systems formed ferritin-Cd, ferritin-As, ferritin-Hg, ferritin-Pb, and ferritin-Cr aggregations. The aggregations of horse spleen ferritin (HSF) and AjFER are relatively unified rules. The enrichment capacity of ferritin was further analyzed using Inductively Coupled Plasma Mass spectrometry. The contents of Cd^{2+}, Hg^{2+}, Cr^{3+}, Pb^{2+}, and As^{3+} enriched by recombinant AjFER were higher than that for the standard HSF in ordinary groups. Moreover, the concentration levels of enriched heavy metal ions in groups treated with phosphate were higher than those in ordinary dialysis control AjFER groups. The conformation stability of AjFER binding to different heavy metal ions was determined using Circular Dichroism (CD) spectroscopy, which revealed that the second structure of M^{n+}-ferritin has relative stability. The affinity of ferritin for metal ions was determined using Isothermal Titration Calorimetry (ITC), and the order of binding constant was Pb-Fer > Hg-Fer > Cd-Fer > As-Fer > Cr-Fer. The ion channel was measured using site-directed mutagenesis, which revealed that heavy metal ions primarily enter the protein cage *via* a three-fold channel and that the ferroxidase center may be one of the key sites for metal ion diffusion into the interior of the protein shell.

Received 23rd June 2017
Accepted 23rd August 2017

DOI: 10.1039/c7ra06989h

rsc.li/rsc-advances

1 Introduction

Heavy metal contamination has become one of the most serious environmental issues in recent years because of the ubiquity, difficult degradation, and easy accumulation of heavy metal pollutants, particularly in the marine environment, which has received global attention. Heavy metals can accumulate in the body and eventually lead to health issues.[1] Heavy metals also threaten littoral and marine surroundings when industrial sewage and sediments are discharged into the ocean.[2,3] In recent years, many techniques for heavy metal elimination have been researched, including chemical and biological methods. Chemical approaches include precipitation,[4] ion-exchange,[5] adsorption,[6] membrane filtration,[7] coagulation flocculation,[8] flotation,[9] and electrochemical[10] methods. However, these approaches often have many limitations, such as high costs, secondary pollution, byproducts, and harsh reaction conditions. The bio-absorption of heavy metals from the environment is a relatively new approach that was shown to be very promising for the elimination of heavy metal ions. These bio-absorption materials include non-living,[11] algal,[12] and microbial[13] biomasses. Despite these materials' inexpensive price and effective adsorption, unfortunately, these studies remain in experimental phases. Moreover, it is difficult to isolate biosorbents after adsorption.

Apostichopus japonicus is a marine animal that belongs to Echinodermata, Holothuroidea, Aspidochirotida, Stichopodidae. *A. japonicus* is primarily detected on the coast of the Yellow Sea and the Bohai Sea in China, which is rich in sea grasses. The water depth in these areas is commonly 3 to 5 meters. Most young *Apostichopus japonicus* live in the intertidal zone or in eelgrass growing on fine sediment bottoms, which have a higher metal ion concentration. Artificially bred *A. japonicus* exist in the bottom of shrimp ponds, where the content of heavy metals is often higher than that in the ocean. Zhang *et al.*[14] studied the effect of Cd^{2+} and Cu^{2+} treatment on ferritin expression, revealing that ferritin mRNA from *Exopalaemon carinicauda* is primarily expressed in the hepatopancreas and that its expression is significantly upregulated at different

[a]*School of Marine Science, Ningbo University, Ningbo, 315211, China. E-mail: suxiurong_public@163.com; luchenyang@nbu.edu.cn; Fax: +86 574 87608368; Tel: +86 574 87608368*

[b]*Department of Food Science, Cornell University, New York, NY, USA*

periods of time after the exposure of shrimp in Cu^{2+} and Cd^{2+} aqueous solution. Liu *et al.*[15] also reported that ferritin expression is associated with heavy metal stimulation. Here, the ferritin gene from *Apostichopus japonicus* was recombined and overexpressed, and the functional characterization of recombinant ferritin was elucidated.

Ferritin is composed of a protein shell with highly symmetrical subunits and of an iron core, which includes thousands of iron phosphate molecules.[16–18] Ferritin is composed of 24 identical monomers, typically with high 432 symmetry. This geometry results in 6 four-fold, 8 three-fold, and 12 two-fold channels. These channels and their nature depend on the subunit type and source.[19] In eukaryotes, the three-fold channel is a hydrophilic channel that connects the internal cavity with the outside environment. There are two three-fold negative amino acid rings situated on the D helix of the ion channel. Calculations of electrostatic surface potential revealed a negative electrostatic funnel that can attract many metal ions, such as Ca, Zn, Mn, Fe, and Mg.[20] The unique shell of ferritin has also been employed as a protein cage to synthesize bionanomaterials.[21,22] The ferritin shell can also be utilized as a template to prepare nanoparticle tags with distinct voltammetric signatures.[23] Under specific *in vitro* conditions, metal compounds (FeS and CdS) and radioactive materials (uranium and nuclear energy) have been successfully assembled into the ferritin nano-space.[22,24–27] In addition, the internal cavity of ferritin can absorb heavy metal ions, such as iron and small organic molecules.[28,29] Heavy metal binding sites are widely distributed throughout the interior and exterior of ferritin, including the inner and outer surfaces of the protein cage, two- and three-phase iron phosphate core surfaces and the deep iron tunnel.[30,31] Thus, ferritin can be used to store excess metal ions in the body and prevent metal ion poisoning.[32,33] Using recombinant ferritin to eliminate heavy metal ions from water can decrease the cost of secondary contamination.[34]

Ferritin can be extracted and purified from animals or plants.[35–37] However, this method is costly and not feasible for large-scale production. The present study aimed to isolate and characterize a new ferritin from the *A. japonicus* cDNA library constructed in our laboratory.[38] Changes in terms of the morphology of the ferritin following heavy metals uptake were determined using scanning electron microscopy (SEM). The ability of isolated ferritin to take up heavy metals under *in vitro* conditions was compared with that of HSF using Inductively Coupled Plasma Mass Spectrometry (ICP-MS). We also evaluated the uptake efficiency of isolated ferritin following phosphate treatment. The secondary structures of refolded AjFER and standard HSF and M^{n+}-AjFER were determined using Circular Dichroism (CD) spectroscopy. The affinity of ferritin for metal ions was also characterized using Isothermal Titration Calorimetry (ITC). The main heavy metal ion channels were roughly confirmed by amino acid site-directed mutagenesis. The present study is expected to provide a foundation for developing a biological material for heavy metal ion removal.

2 Materials and methods

2.1 Expression and purification of *A. japonicus* ferritin

Ferritin cDNAs from *A. japonicus* were cloned in a previous study,[38] a cDNA encoding full-length AjFER were identified and characterized by using approaches such as cDNA library preparation, rapid amplification of cDNA ends, fluorescence real-time quantitative polymerase chain reaction (PCR), and western blotting. AjFER cDNA was 1222 bp in length and comprised a 513-bp 5′-UTR containing a putative iron regulatory element, a 187-bp 3′-UTR, and a 522-bp complete open reading frame encoding a polypeptide with 173 amino acid residues. The conserved motifs of ferritin, including iron binding signature, H-specific ferroxidase center, and phosphorylation site, were present in the deduced amino acid sequence of AjFER. A PCR fragment encoding the mature polypeptide of AjFER was amplified using gene-specific primers Fer-R (5′-GGATC CATGCAGCCAAGCCAAGTC-3′) and Fer-F (5′-AAGCTTTTAATC CTCCTTCAGGTT-3′), both of which contained BamHI and HindIII sites at their 5′ ends. The PCR products were cloned into a pMD18-T vector (TakaRa), digested using restriction enzymes BamHI and HindIII (NEB), and subcloned into the BamHI/HindIII sites of pET-28a(+) expression vector (Novagen). The recombinant plasmid (pET-28a-AjFER) was transformed into *Escherichia coli* BL21 cells (Novagen). Positive clones were identified by kanamycin screening and sequencing. The recombinant plasmid (pET-28a-AjFER) was transformed into *Escherichia coli* BL21. *A. japonicus* ferritin was also expressed and purified.[39] A positive clone was incubated overnight at 37 °C at 120 rpm, and after the culture reached an $OD_{600} = 0.6$ to 0.8, 1 mM isopropyl β-D-thiogalacto-pyranoside (IPTG) was added to induce AjFER expression for an additional 12 h. Ferritin was purified using a Ni-NTA affinity column. The expression and purified products were further incubated in GSH/GSSG buffer (50 mM Tris–HCl, 1 mM EDTA, 50 mM NaCl, 10% glycerol, 1% glycine, 2 mM reduced glutathione, and 0.2 mM oxide glutathione, pH 8.0) with a stepwise decrease of urea with the order of 6 M, 4 M and 2 M overnight at 4 °C to promote purified protein refolding and obtain AjFER with biological activity. The obtained activated AjFER was incubated in buffer solution (25 mmol L^{-1} Tris–HCl, 150 mmol L^{-1} NaCl, pH 8.0) with 0.5 U mg^{-1} thrombin at 25 °C for 2 h so as to remove the his-tag. Enzyme-digested products was separated by Sephacryl S-300 HR column equilibrated with 150 mmol L^{-1} NaCl at pH 8.0. The collected AjFER was examined by SDS-PAGE.

2.2 Functional characterization of AjFER

Ordinary heavy metals treatment. To determine the heavy metal uptake capacity, 2 mL of AjFER and 2 mL of horse spleen ferritin (HSF) (Sigma, Beijing, China) (20 mg mL^{-1}) were dialyzed with 100 mL of 2 mM $CdCl_2$, $HgCl_2$, $CrCl_3$, $Pb(NO_3)_2$, and $AsCl_3$ (pH 5.5) at 4 °C for 12 h, according to the preliminary experiments. Subsequently, 2 mL of each mixture was dialyzed in 10 mM 2-morpholinoethanesulfonic acid (MES) to remove the heavy metal ions that were not adsorbed. The liquid flows

were maintained using a magnetic stirrer, and the solution was replaced once every 4 h.

Phosphate stimulation. AjFER and HSF were dialyzed with a 100-mL solution containing 2 mM $CdCl_2$, $HgCl_2$, $CrCl_3$, $Pb(NO_3)_2$, and $AsCl_3$ (pH 5.5) for 12 hours, then replaced with 2 mM phosphate buffer saline (PBS), and finally dialyzed with a solution containing 10 mM MES and 150 mM NaCl, pH 5.5, to remove the unabsorbed heavy metal ions.

2.3 SEM analysis

AjFER and HSF treated with five metal ions were evenly smeared onto the surface of pretreated mica sheets and dried for 4 days at room temperature (environmental humidity, 5%).[39] The surface morphologies were observed using scanning electron microscopy (SEM) (S-3400N, Hitachi, Japan) with a 40-mm probe distance, 30° sample inclination, 21-mm working distance, and 100-s analysis time.

2.4 ICP-MS analysis

A total of 15 ferritin groups (ten ordinary groups and five phosphate-stimulated groups) enriched with heavy metals were collected from dialysis and each group was subjected to five repeated trials. The concentration of ferritin sample was determined by using BCA kit (Sangon, Shanghai, China). For microwave digestion, 1 mL of each ferritin sample was accurately transferred directly to a polytetrafluoroethylene digestion vessel. The micro-wave digestion parameters were based on our previous work.[39] Sample blanks were also prepared using the aforementioned full analytical procedure, except for sampling and analysis. The calibration standard solutions were prepared using a 10 mg L^{-1} multi-element standard solution (CLMS-2AN, Spex, CA, USA). All reagents were of analytical grade or better. For sample dilution and preparation of the standards, we used ultrapure water (MilliQ, Millipore). The data were then subjected to one-way analysis of variance (ANOVA). Differences were considered significant at $P < 0.05$. The molar ratio of metal ions *vs.* ferritin (M^{n+}/protein) can be calculated since the contents of metal ions binding to Ajfer per unit volume can be determined by ICP-MS, and the contents of AjFER per unit volume can be determined by BCA kit.

2.5 Circular dichroism analysis

CD was performed using a JASCO J-815 CD spectrophotometer in the far UV range of 260–190 nm at room temperature using a 0.1 cm quartz cuvette. The obtained results were analyzed using the CDPro software, and the proportions of α-helices, β-sheets, β-turns and unordered conformations in the protein were obtained.

2.6 Isothermal titration calorimetry analysis

High-sensitivity ITC experiments were conducted at 25 °C using a MicroCal ITC200 (Malvern Instruments). The M^{n+} solution was prepared in a buffer containing 25 mM MES, pH 5.5, and 150 mM NaCl. A large number of pre-experiments of titration of metal ions to ferritin was performed so as to obtain the suitable titration concentration, since it is a complex binding reaction of metal ions binding to ferritin. The final concentrations of Cd^{2+}, Cr^{3+}, As^{3+}, Pb^{2+}, and Hg^{2+} were 16.7 mM, 2.5 mM, 2.5 mM, 556 μM, and 800 μM, respectively. AjFER was used at concentrations of 2.5, 0.5, 5, 0.25, and 0.5 μM, respectively. M^{n+} was titrated into the protein solution in a series of 19 injections of 2 μL (the first injection was a dummy injection of 0.4 μL), at 2 min apart, with a stirring speed of 750 rpm. All data analysis has been performed using Origin Pro version 8.0.[40]

2.7 Preparation of mutants

In a previous study, the ferroxidase center sites and ion channels were predicted using the SMART procedure.[38] The results indicated that the ferroxidase center was composed of Glu-25, Tyr-32, Glu-59, Glu-60, His-63, Glu-105, and Gln-139, and the ion channels was composed of His-116, Asp-129, and Glu-131. The mutant ferroxidase center (S1) (E25A, Y32A, E59A, E60A, H63A, E105A, and Q139A) and ion channels (S2) (H116A, D129A, and E131A) were prepared using gene synthesis.

3 Results

3.1 Recombinant expression of AjFER

The lysate was analyzed using SDS-PAGE. Obvious protein bands with a molecular weight of 24 kDa were detected after IPTG induction (Fig. 1A and B) and could be purified to homogeneity using HiTrap Chelating Columns. The result was consistent with the theoretical molecular mass of a subunit. Moreover, the content of overexpressed recombinant ferritin increased with time. The expression of recombinant ferritin peaked at 5 h after adding IPTG to the culture. A single protein band was observed after purification using Ni-NTA. Native-PAGE was used to characterize the multi-subunit refolding and recombination (Fig. 1C). A protein band with a molecular weight of 576 kDa was observed in lane 1, indicating that 24 monomers were packed together. As treated with thrombin, the His-tage was removed from obtained overexpressed ferritin. A protein band with a molecular weight of 20 kDa was observed in lane 2, indicating that His-tage were removed from ferritin (Fig. 1D).

3.2 Morphological characterization of recombinant ferritin following different treatments

As shown in Fig. 2A, the aggregation of recombinant AjFER in the negative group exhibited divergent spherical shapes with cage-like morphologies. The HSF aggregated close together, forming a lattice (Fig. 2B). Each HSF aggregate in the negative group was similar, with sizes ranging from 1 to 2 μm. In contrast to HSF, the AjFER aggregates were approximately 5 μm in size. After treatment with different heavy metals, the surface morphology of the HSF and AjFER aggregates changed dramatically. Different metals resulted in different surface morphologies. In the Hg^{2+} treatment groups (Fig. 2C and D), the aggregation monomers of HSF and AjFER adhered together like a honeycomb. The edge shapes of the aggregation were fuzzy. The two kinds of ferritin aggregations exhibited adhesion in

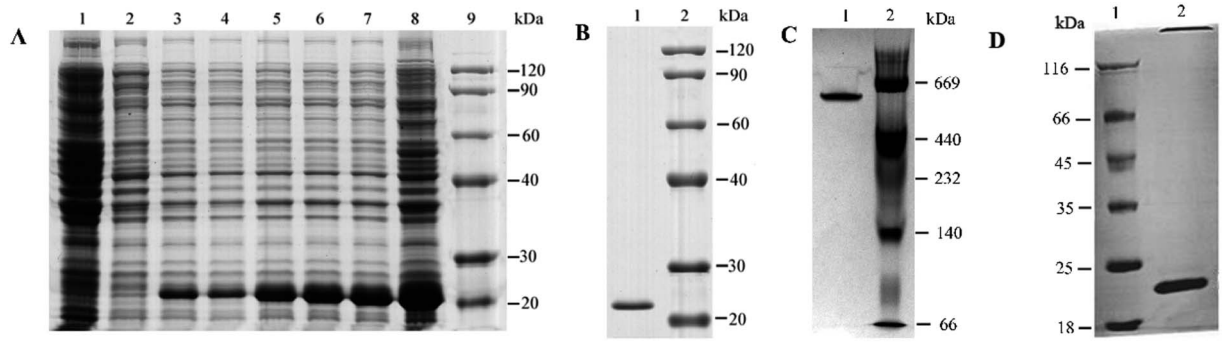

Fig. 1 Expression and purification of pET-FER recombinant AjFER protein in *E. coli* BL21. (A) Lane 1: total protein of pET-28a induced for 5 h, lane 2: total protein of non-induced pET-FER, lanes 3–8: total protein of pET-FER induced for 1, 2, 3, 4, 5, and 12 h, lane 9: middle molecular marker; (B) lane 1: purified protein of pET-FER, lane 2: middle molecular marker. (C) Lane 1: purified native protein of PET-FER, lane 2: high molecular weight marker. (D) Lane 1: middle molecular marker, lane 2: purified protein of pET-FER without His-tage.

a honeycomb shape after absorbing Cr^{3+} (Fig. 2E and F). The edge of the aggregation was not obvious. Aggregations with larger monomer sizes gathered into a honeycomb with holes containing an extensive amount of small ferritin aggregations. In the Pb^{2+} treatment groups (Fig. 2G and H), the ferritin aggregates were ellipsoid with non-uniform sizes. Some of the aggregate adhered together, also with a single aggregate. In the As^{3+} treatment groups (Fig. 2I and J), the aggregates formed an irregular block layer, which adhered to the surface of irregular similar layers. Compared to HSF, the coverage of recombinant AjFER aggregations was more intense in the five metal treatment groups. In addition, the aggregations were larger in the Pb^{2+} treatment groups than in groups treated with other metals. In the Cd^{2+} treatment groups (Fig. 2K and L), the aggregates of HSF and AjFER were present in the form of small and uniform sphere piles.

3.3 Quantitative analysis to determine heavy metal enrichment capacity

ICP-MS analysis was used to further confirm the content of heavy metal elements enriched by AjFER. As shown in Fig. 3, in the AjFER groups, the content enrichment order from high to low was $Cd^{2+} > As^{3+} > Hg^{2+} > Pb^{2+} > Cr^{3+}$. In the HSF group, the enrichment order from high to low was $Cd^{2+} > As^{3+} > Hg^{2+} > Cr^{3+} > Pb^{2+}$. The enrichment of the five heavy metals in recombinant AjFER was higher than that in standard HSF ($P < 0.01$) in the ordinary group. The concentration of heavy metals in the ordinary dialysis control groups was lower than that in the phosphate-stimulated groups ($P < 0.05$). The contents of Cd, As, Hg, Pb and Cr in ordinary groups are 1139.5, 234.2, 87.8, 84 and 8.2, respectively. While the enrichment of metal ions increased obviously in phosphate-stimulated group and the contents are 1566.7, 507.5, 148.1, 141.3 and 25.8, respectively. The PBS may contribute to form the metal ion core that attract more metal ion entering into the inner of protein cage.

3.4 Secondary structure determination

To further describe the conformational changes of ferritin in the presence of heavy metal ions, CD spectra were examined. As shown in Table 1, the contents of the secondary structure in the native AjFER group were similar to those of the HSF group, indicating that recombined AjFER has a similar secondary structure. Cd-AjFER, Cr-AjFER, As-AjFER, Pb-AjFER, and Hg-AjFER were also prepared and the contents of the secondary structure show that the main variations were observed among α-helices, β-turns, and random coils. The number of α-helices in the treatment group decreased, whereas the number of random coils generally increased compared with the native ferritin group, indicating a change in conformation, possibly because the α-helices transformed into random coils. Among the treatment groups, there were also differences in the secondary structure, indicating that metal species have different influences on structures. In particular, the conformation of Pb-AjFER changed the most, for which the β-sheet increased by 13.1% and the random coils decreased to 19.3% from 28.3%, suggesting that Pb^{2+} has a larger effect on AjFER.

3.5 ITC of M^{n+} binding to AjFER

Isothermal titration calorimetry (ITC) has widely been used to measure interactions between metal ions and biomolecules, such as amino acids, peptides, and protein.[41–43] ITC is the most quantitative technique used to determine the thermodynamic properties of any biochemical reaction. The raw data from Fig. 4 show an exothermic reaction of Cd^{2+}, Pb^{2+}, Hg^{2+}, As^{3+}, and Cr^{3+} binding to AjFER, as negative peaks correspond to an endothermic reaction. This finding was also reflected by the negative enthalpy value shown in Table 2. Gibbs free energy (ΔG) was calculated to represent the direction of the reaction. The value of ΔG in Table 1 was negative, indicating a spontaneous reaction favorable for the combination of protein with metal ions. Fig. 4A shows an apparent two-inflection point. Accordingly, a model of two sets of independent binding sites was used to fit a curve to the data for Cd-AjFER. For Cd-AjFER, both strong and weak binding classes were observed with AjFER (Fig. 4A, Table 2). The stoichiometry of the strong binding class was ~11 molar equivalents per protein, and the weak binding class was ~39 molar equivalents per protein. The other metal ions showed only one inflection point, and the data for the other metal ions

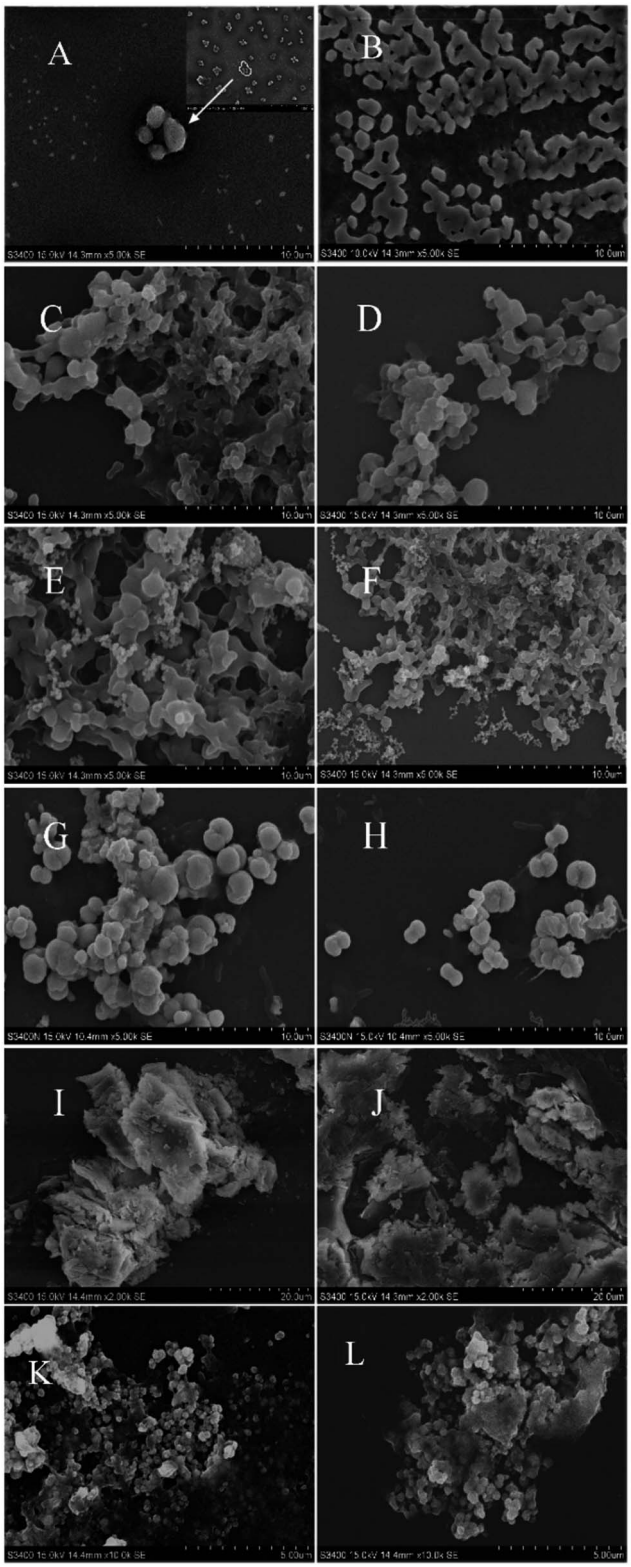

Fig. 2 SEM of different treatment groups. (A) The negative control of AjFER without metal treatment; (B) the negative control of HSF without metal treatment. (C) AjFER with Hg^{2+} treatment; (D) HSF with Hg^{2+} treatment; (E) AjFER with Cr^{3+} treatment; (F) HSF with Cr^{3+} treatment; (G) AjFER with Pb^{2+} treatment; (H) HSF with Pb^{2+} treatment; (I) AjFER with As^{3+} treatment; (J) HSF with As^{3+} treatment; (K) AjFER with Cd^{2+} treatment; (L) HSF with Cd^{2+} treatment.

were used to curve fit a model of one set of independent binding sites (Fig. 4B–E). The derived parameters for the binding sites of different metal ions are summarized in Table 2. The binding constant is used to characterize the affinity between metal ions and proteins. Table 2 shows obvious affinity differences of M^{n+}-FER, with the following order: Pb-Fer > Hg-Fer > Cd-Fer > As-Fer > Cr-Fer. These results suggest a strong affinity of AjFER to Pb^{2+} and a relatively weak affinity of AjFER to Cr^{3+}. The binding constant of Cd-Fer was close to that of As-Fer. These results are consistent with the observed changes in secondary structure.

3.6 M^{n+} binding to AjFER variants

Ferritin is composed of 24 identical subunits, forming a caged structure with an internal diameter of 8 nm, which can accommodate ~3500 ions. The arrangement of subunits forms three small molecule channels, including a two-fold channel, a three-fold channel, and a four-fold channel, on the surface of the protein cage. In eukaryotes, the three-fold channel is the main protein cage for small molecules.[44,45] To further verify the ion channel and location of heavy metal ion binding to protein, in the present study three-fold-symmetry channel variants (S1) and ferroxidase center variants (S2) were prepared. The over-expressed and purified variants and native AjFER (control group) were treated with five metal ions under the same conditions. As shown in Fig. 5, the metal ion enrichment of variant S1 was obviously decreased compared with the control group ($P < 0.01$), suggesting that three-fold channels are the main channels of heavy metal ion sequestration into the protein cage. The content of the five metal ions binding to variant S2 also decreased ($P < 0.05$), suggesting that the ferroxidase center can bind metal ions.

4 Discussion

The binding activity of AjFER for different heavy metals was investigated using scanning electron microscopy (SEM) because of the sensitivity and selectivity of this technique.[46–49] After purifying recombinant AjFER, the vast majority of subunits in AjFER were detected as free peptide chains. Inclusion bodies solubilized in the presence of urea were diluted with denaturation solution, and the bioactive recombinant AjFER was released. The morphology of recombinant AjFER and natural HSF was similar. The shapes of some ferritin aggregations were irregular, with a small amount of ferritin fragments. The addition of metal ions, as a result of combinations with metal ligands and interactions between amino acid side chains, such as hydrophobic bonding, hydrogen bonding, van der Waals force and electrostatic effects, significantly influenced ferritin folding.[26,50,51] These factors gradually increased the number of subunits constituting ferritin, thereby increasing the thickness of the protein shell. Several space changes were observed in ferritin, with the surfaces forming several large gaps. However, metal ion hydrations may destroy the ferritin hydration layer, making ferritin intermediates easier to fold. The stronger the metal ion hydration, the greater the role in promoting the

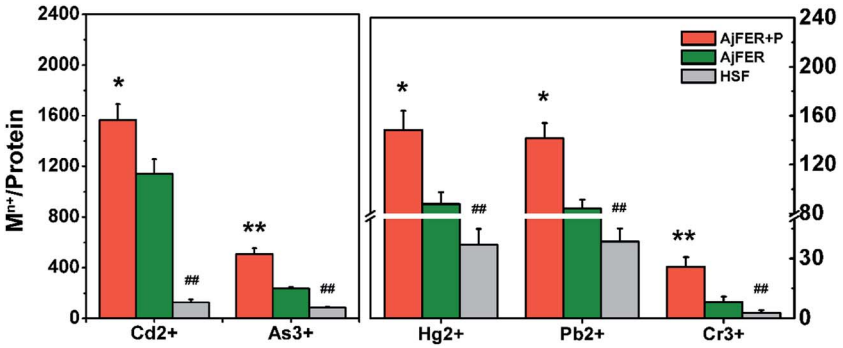

Fig. 3 Contents of different metal ions in AjFER, AjFER + P, and HSF. AjFER + P: phosphate-stimulated AjFER. Metal ions concentration was determined by ICP-MS and protein concentration was determined by BCA kit. Each symbol and vertical bar represents the means ± the S.D. (n = 5). Data are expressed in terms of the means ± the S.D. *P < 0.05, **P < 0.01 AjFER + P group *vs.* AjFER group. ##P < 0.01 HSF group *vs.* AjFER.

Table 1 The secondary structure contents of ferritins with and without heavy metal ions

	Secondary structure contents (%)						
Categories	HSF	AjFER	AjFER-Cd	AjFER-Cr	AjFER-As	AjFER-Pb	AjFER-Hg
α-Helix	25.9	34.5	31.6	32	27.4	32.7	28
β-Sheet	0	0	0	0	0	13.1	0
β-Turn	32.5	37.2	37.3	38.1	33.3	34.9	33.4
Random coils	41.5	28.3	31.1	30	39.3	19.3	38.6

formation of ferritin metal aggregations. Eventually, the reaction systems formed ferritin-Cd, ferritin-As, ferritin-Hg, ferritin-Pb, and ferritin-Cr aggregations.

The ICP-MS technique has widely been used for the determination of metal elements because of its high level of sensitivity and capability for multi-element analysis.[52–54] ICP-MS has commonly been used to determine the geographic origin of medicinal herbs, minor and trace elements in aromatic spices, and agricultural crops.[55–57] In this study, AjFER was expressed and purified based on a previous study, and then, the recombinant ferritin was characterized according to enrichment level after exposure to different heavy metals. The heavy metal elements enriched by AjFER were analyzed using ICP-MS to better understand the role of the AjFER in heavy metal detoxification.

The bioactive *Apostichopus japonicus* ferritin was obtained using a restructuring technique. AjFER absorbed several types of heavy metals, and the concentrations of different metals were all greater than those of horse spleen ferritin. The flexible adjustment of the ferritin protein shell and the combination of the close degree between protein subunits play important roles in the physiological functions of ferritin.[58–60] Recombinant AjFER, without iron core framework support, may be more flexible and show increased plasticity, thus providing more enrichment of heavy metals. Different heavy metal ions have different atomic radius sizes, and the numbers of nuclei are also different. Moreover, when the metal ions pass through ferritin ion channels, the different valences and redox abilities may cause different changes in internal ferritin factors.[33,50] These factors could lead to different metal ion concentration levels.

Iron absorption and ferritin release are controlled by the complex phosphorus iron structure on the surface of the iron core.[61–63] The rate of iron release is associated with the reducing agent and formation of the iron core.[61] Medium H^+ and OH^- not only participate in the composition of the iron core but also combine with amino acids on the inside and outside of the protein shell surface, thus affecting the conformation and the flexible adjustment ability of the protein shell.[33] The phosphate groups distributed throughout the ferritin shell increase the electrostatic repulsion between protein molecules, enabling more favorable dispersion in solution.[64] In addition, the metal phosphate seed is an auto-catalyst, and metal phosphate will be rapidly developed in the ferritin cage.[23] Our results were consistent with the theory that recombinant AjFER, which is more flexible and shows more plasticity, is more attractive to heavy metal ions than HSF. Phosphate stimulation can increase the concentration of metal ions in AjFER compared with the ordinary dialysis control groups.

Circular dichroism is a spectroscopic technique that is broadly used for assessing macromolecular interactions and conformational changes in solution.[65,66] In this study, we determined the secondary structure of ferritin after refolding, using standard HSF as a comparison sample. The results suggest that activated AjFER can be obtained using a stepwise decrease of urea. Because of its corrected secondary structure, Native-PAGE revealed that 24 subunits were successfully packed together through intermolecular forces. The metal-ferritin conformation was also examined using CD spectroscopy. The results showed that the α-helices in the metal ion-treated group decreased. It is likely that the metals bound to ferritin may shift

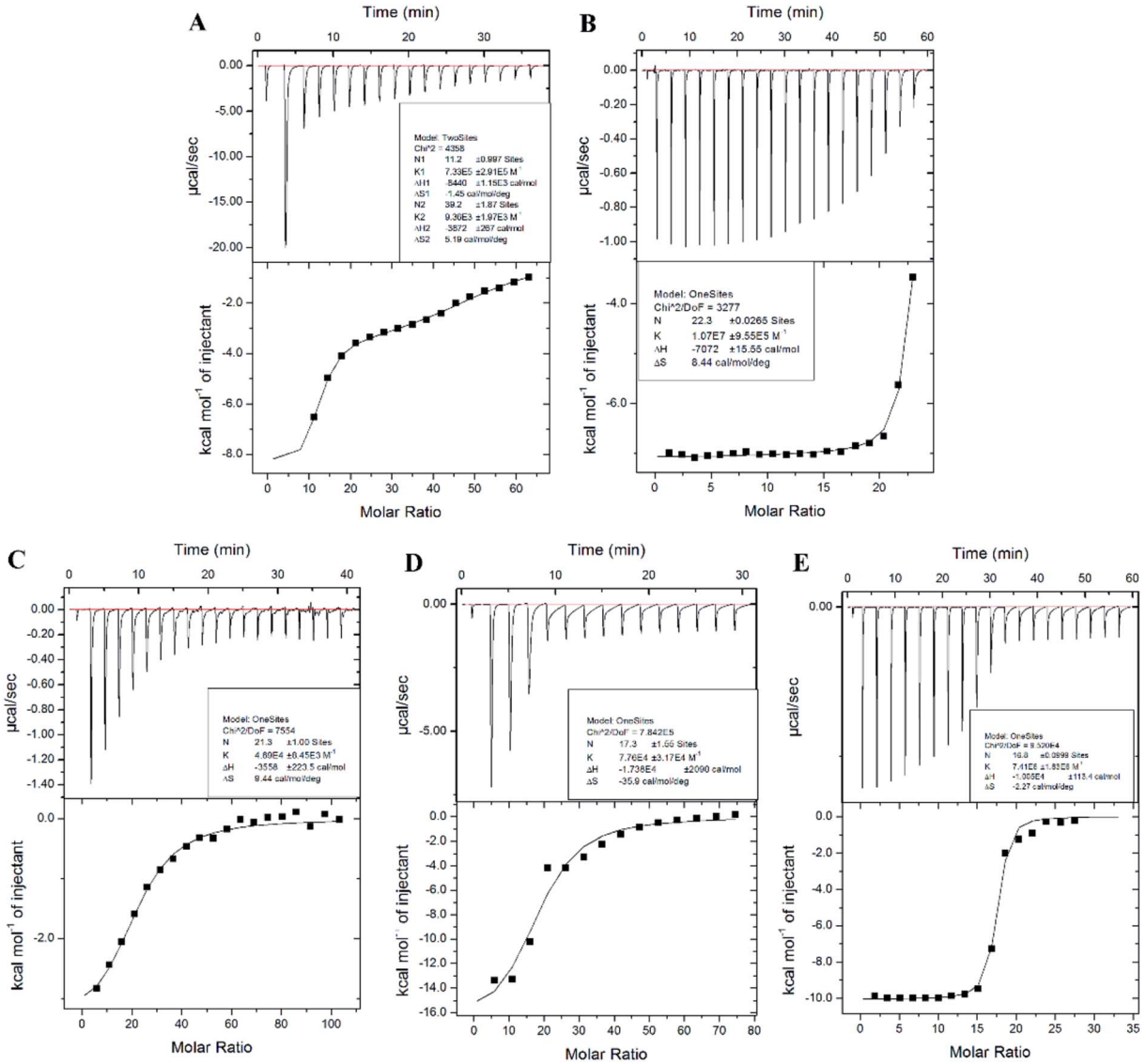

Fig. 4 The calorimetric titration isotherms of the binding interaction between M^{n+} and apo-AjFER in 25 mM MES buffer, pH 5.5, at 298.15 K. (A) 2.5 μM AjFER titrated with 38.4 μL injections of 16.7 mM $CdCl_2$; (B) 0.25 μM AjFER titrated with 38.4 μL injections of 0.556 mM $Pb(NO_3)_2$; (C) 0.5 μM AjFER titrated with 38.4 μL injections of 2.5 mM $CrCl_3$; (D) 5 μM AjFER titrated with 38.4 μL injections of 2.5 mM $AsCl_3$; (E) 0.5 μM AjFER titrated with 38.4 μL injections of 0.8 mM $HgCl_2$.

Table 2 Best fit parameters for ITC measurements of M^{n+} binding to apo-AjFER at 25 °C

Protein	N	Ka (M^{-1})	ΔH^0 (cal mol^{-1})	ΔS^{0a} (cal mol^{-1} deg^{-1})	ΔG_1^{0b} (kJ mol^{-1})
Cd-Fer	N1: 11.2 ± 0.997	Ka1: $7.33 \times 10^5 \pm 2.91 \times 10^5$	ΔH^1:-8440 ± 1150	ΔS^1:-1.45	−8007.68 ± 1150
	N2: 39.2 ± 1.87	Ka2: $9.36 \times 10^3 \pm 1.97 \times 10^3$	ΔH^2:-3872 ± 267	ΔS^2:5.19	−5419.4 ± 267
Pb-Fer	22.3 ± 0.0265	$(1.07 \pm 0.0955) \times 10^7$	−7072 ± 15.55	8.44	−9588.39 ± 15.55
Cr-Fer	21.3 ± 1.00	$(4.69 \pm 0.845) \times 10^5$	−3558 ± 223.5	9.44	−6372.54 ± 223.5
As-Fer	17.3 ± 1.55	$(7.76 \pm 3.17) \times 10^4$	$-1.738 \times 10^4 \pm 2090$	−35.9	−6676.42 ± 2090
Hg-Fer	16.8 ± 0.0999	$(7.41 \pm 1.83) \times 10^6$	$-1.005 \times 10^4 \pm 113$	−2.27	−9373.2 ± 113

[a] Calculated from $\Delta S = (\Delta H - \Delta G_1^0)/T$. [b] Calculated from $\Delta G_1^0 = -RT \ln K$.

the ferritin conformation toward disordered. Ferritin cages are formed by arrays of self-assembling four-helix bundles,[67] and metal ion binding sites are primarily located on α-helices in ferritin, as revealed in the crystal structure.[67–69] Heavy metal ion binding with amino acid residues on helices may be the main reason for the decrease in α-helices. For Pb-AjFER, the β-sheet

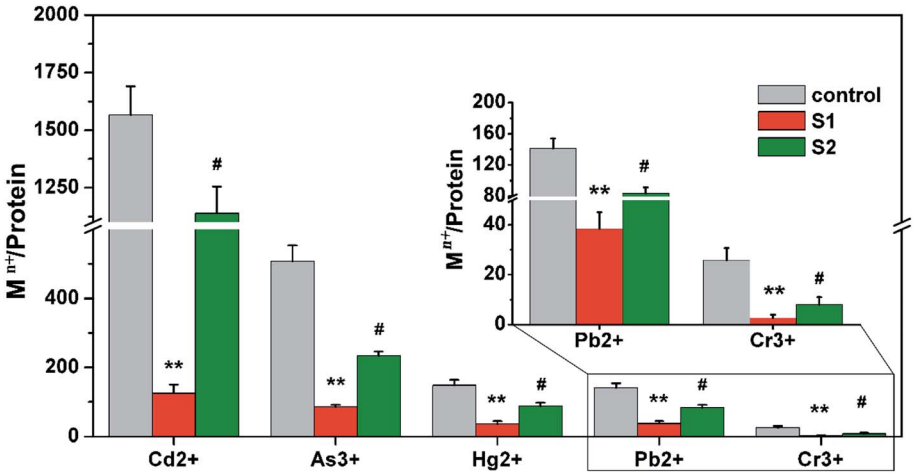

Fig. 5 Contents of different metal ions in native ferritin, a three-fold channel variant and the ferroxidase center treated with different metal ions. Metal ions concentration was determined by ICP-MS and protein concentration was determined by BCA kit. Control represents native AjFER, S1 represents the three-fold channel variant, and S2 represents the ferroxidase center. Data are expressed in terms of the means ± the S.D. $^{**}P <$ 0.01 S1 group *vs.* control group. $^{\#\#}P <$ 0.01 S2 group *vs.* control group.

showed an obvious increase. This inconsistency may be attributed to the properties and binding sites of Pb^{2+}, as changes in the microenvironment near binding sites promote β-sheet formation. Harshith Subramanian *et al.*[66] investigated the effect of Cu^{2+} and Mn^{2+} on horse spleen apoferritin, revealing that the number of β-sheets changed in response to treatments with different metal ion species and at different concentrations. We readily admit that only a secondary structure measurement, as found here, may not fully reflect the binding mechanism of metal ions and protein. Protein crystallization is needed to determine the binding sites in the protein cavity.

The stoichiometry of metal ion binding to AjFER determined using ITC is inconsistent with results from ICP-MS above. The stoichiometry of metal ions binding to AjFER determined using ITC is inconsistent with results from ICP-MS. In study of ITC, the stoichiometry of Cd, As, Hg, Pb and Cr binding to AjFER was 50.4, 17.3, 16.8, 22.3 and 21.3, respectively. While the results of ICP-MS indicated that the stoichiometry of Cd, As, Hg, Pb and Cr are 1139.5, 234.2, 87.8, 84 and 8.2, respectively. There are two possible reasons to account for this case. First, most metal ions entering the cavity are in a free state. These metal ions do not or only indirectly bind to amino acid residues, producing little heat change. Enthalpy changes from second- and third-class binding sites are too weak to be fitted to a curve. Thus, the stoichiometry shown in Table 2 may mainly represent first-class binding sites. Second, one binding site may capture more than one metal ion, such as the formation of a gold cluster.[68,70] The stoichiometries of Pb^{2+} and Cr^{3+} are approximately 22 and 21, respectively. Thus, these binding sites may be located in 24 subunits, suggesting the existence of a binding site in each subunit. In addition, the ΔS from Pb-Fer and Cr-Fer showed positive values, suggesting that the change occurred due to a hydrophobic interaction. Thus, these interactions were most likely located in the 24 subunits of the ferroxidase center. The stoichiometry of Cd^{2+}, As^{3+}, and Hg^{2+} are 11, 17, and 17, respectively, implying metal ion binding to eight three-fold channels with relatively strong binding, and approximately two metal atoms in each three-fold channel. Bou-Abdallah *et al.*[71] examined the affinity of ferritin to Zn(II) and Tb(III) using ITC, revealing that three-fold channels in ferritin strongly adsorb Zn(II) and Tb(III) and the ferroxidase center weakly adsorbs Zn(II) and Tb(III). This inconsistence may be caused by the different properties of different metal ions and different microenvironments of different proteins. Since ITC directly measures the total heat flow, all processes occurring upon the addition of the titrant will contribute to the measured enthalpy. Therefore, the details of heat contribution from specific amino acid residues should be described using protein crystallization technology and site-directed mutagenesis in future studies.

Many mutagenesis studies in terms of ferritin have been performed.[72–74] Wade *et al.* prepared glutamic acid residue mutagenesis in the shell of human ferritin and assessed their role in iron core development.[73] In this study, the mutagenesis of key amino acid residues inside the ferritin cage was conducted, and their roles were explored. Here, we found that heavy metal ions penetrate into the ferritin shell *via* three-fold channels where amino acids H116, D129, and E132 are located. These amino acids residues play crucial roles in metal ion adsorption. The channel is composed of two three-fold highly conserved negative amino acid rings. The three Asp residues from three different subunits form the inner layer close to the shell interior, and three Glu residues form the middle layer in the ferritin shell before funnel opening. Calculations of the electrostatic surface potential indicated the existence of a negative electrostatic funnel that allows the attraction and insertion of many divalent ions, such as Fe, Ca, Zn, Mg, and Mn.[20] Molecular diffusion research in human heavy chain ferritin and horse spleen ferritin verified this finding and elucidated the penetrability of the ferritin cavity to small molecules *via* the three-fold channels.[44,45] A thermodynamic

study in terms of three-fold channel mutants has verified an iron ion channel in the cavity, indicating that the binding ability for Fe^{2+} decreased.[41] The ferroxidase center is composed of two iron sites, FeA, including Glu-27, Glu-65, and His-62, and FeB, including Glu-107 and Glu-62. In this study, theoretically, the amount of metal ions bound to the ferroxidase center variant should decrease by 48 metal atoms per mutant cage at most. Notably, the amount of metal ions was reduced by more than 48, with the exception of Cr^{3+}. These results indicate that ferroxidase center sites may contribute to metal ion migration from the entrance of three-fold channels to the inner protein cavity.

5 Conclusions

We characterized recombinant AjFER from *Apostichopus japonicus* with heavy metal detoxification activity. This study indicated that AjFER showed an advantage in the enrichment capacity of Cd^{2+}, Hg^{2+}, Cr^{3+}, Pb^{2+} and As^{3+} compared with standard HSF. In addition, the content of heavy metals showed a marked increase in phosphate-stimulated groups over the control group. The affinity of ferritin to different heavy metal ions was Pb-Fer > Hg-Fer > Cd-Fer > As-Fer > Cr-Fer. The heavy metal ions primarily entered the ferritin shell *via* three-fold channels composed of three key amino acid residues H116, D129, and E132. The ferroxidase center, including E25, Y32, E59, E60, H63, E105, and Q139, contribute to the enrichment of heavy metal ions. These studies provide a significant theoretical basis for the development of materials for heavy metal ion removal.

Conflicts of interest

There are no conflicts to declare.

Acknowledgements

This work was supported by the National Natural Science Foundation of China (No. 41176123, No. 40776075 and No. 41676159) and the K. C. Wong Magna Fund of Ningbo University. Our ITC work was performed at the National Center for Protein Science Shanghai.

References

1 J. A. Cooke, S. M. Andrews and M. S. Johnson, *Water, Air, Soil Pollut.*, 1990, **51**, 43–54.
2 K. Pan and W. X. Wang, *Sci. Total Environ.*, 2012, **421–422**, 3–16.
3 G. Zhang, D. Liu, H. Wu, L. Chen and Q. Han, *Ecotoxicology*, 2012, **21**, 1726–1733.
4 Y. Ku and I. L. Jung, *Water Res.*, 2001, **35**, 135–142.
5 S. Y. Kang, J. U. Lee, S. H. Moon and K. W. Kim, *Chemosphere*, 2004, **56**, 141–147.
6 A. Jusoh, L. S. Shiung, N. A. Ali and M. J. M. M. Noor, *Desalination*, 2007, **206**, 9–16.
7 J. Landaburu-Aguirre, V. García, E. Pongrácz and R. L. Keiski, *Desalination*, 2009, **240**, 262–269.
8 A. E. Samrani, B. S. Lartiges and F. Villiéras, *Water Res.*, 2008, **42**, 951–960.
9 F. Tessele, M. Misra and J. Rubio, *Miner. Eng.*, 1998, **11**, 535–543.
10 I. Heidmann and W. Calmano, *J. Hazard. Mater.*, 2008, **152**, 934–941.
11 F. Kaczala, M. Marques and W. Hogland, *Bioresour. Technol.*, 2009, **100**, 235–243.
12 R. Apiratikul and P. Pavasant, *Bioresour. Technol.*, 2008, **99**, 2766–2777.
13 M. Tuzen, K. O. Saygi, C. Usta and M. Soylak, *Bioresour. Technol.*, 2008, **99**, 1563–1570.
14 J. Zhang, T. Gui, J. Wang and J. Xiang, *Int. J. Biol. Macromol.*, 2015, **72**, 320–325.
15 Q. N. Liu, Z. Z. Xin, Y. Liu, Z. F. Wang, Y. J. Chen, D. Z. Zhang, S. H. Jiang, X. Y. Chai, C. L. Zhou and B. P. Tang, *Fish Shellfish Immunol.*, 2017, **63**, 297–303.
16 G. C. Ford, P. M. Harrison, D. W. Rice, J. M. A. Smith, A. Treffry, J. L. White and J. Yariv, *Philos. Trans. R. Soc., B*, 1984, **304**, 551–565.
17 S. C. Andrews, P. M. Harrison, S. J. Yewdall, P. Arosio, S. Levi, W. Bottke, M. V. Darl, J. F. Briat, J. P. Laulhère and S. Lobreaux, *J. Inorg. Biochem.*, 1992, **47**, 161–174.
18 P. D. Hempstead, S. J. Yewdall, A. R. Fernie, D. M. Lawson, P. J. Artymiuk, D. W. Rice, G. C. Ford and P. M. Harrison, *J. Mol. Biol.*, 1997, **268**, 424–448.
19 R. R. Crichton and J. P. Declercq, *Biochim. Biophys. Acta*, 2010, **1800**, 706–718.
20 F. Bouabdallah, G. Zhao, G. Biasiotto, M. Poli, P. Arosio and N. D. Chasteen, *J. Am. Chem. Soc.*, 2012, **130**, 17801–17811.
21 F. C. Meldrum, B. R. Heywood and S. Mann, *Science*, 1992, **257**, 522–523.
22 T. Douglas, D. P. Dickson, S. Betteridge, J. Charnock, C. D. Garner and S. Mann, *Science*, 1995, **269**, 54–57.
23 G. Liu, H. Wu, A. Dohnalkova and Y. Lin, *Anal. Chem.*, 2007, **79**, 5614–5619.
24 F. C. Meldrum, V. J. Wade, D. L. Nimmo, B. R. Heywood and S. Mann, *Nature*, 1991, **349**, 684–687.
25 S. Pead, E. Durrant, B. Webb, C. Larsen, D. Heaton, J. Johnson and G. D. Watt, *J. Inorg. Biochem.*, 1995, **59**, 15–27.
26 K. Y. Kim, Y. L. Sang, Y. S. Cho, I. C. Bang, K. H. Kim, S. K. Dong and Y. K. Nam, *Fish Shellfish Immunol.*, 2007, **23**, 1043–1059.
27 T. Rakshit and R. Mukhopadhyay, *J. Colloid Interface Sci.*, 2012, **388**, 282–292.
28 C. Li, Z. Li, Y. Li, J. Zhou, C. Zhang, X. Su and T. Li, *PLoS One*, 2012, **7**, e51428.
29 Y. Lu, A. Zhang, C. Li, P. Zhang, X. Su, Y. Li, C. Mu and T. Li, *Fish Shellfish Immunol.*, 2013, **35**, 271–277.
30 A. Treffry, P. M. Harrison, A. Luzzago and G. Cesareni, *FEBS Lett.*, 1989, **247**, 268–272.
31 D. M. Lawson and J. M. Smith, *Nature*, 1991, **349**, 541.
32 P. Arosio, R. Ingrassia and P. Cavadini, *Biochim. Biophys. Acta*, 2009, **1790**, 589–599.
33 R. J. Hilton, B. Zhang, L. N. Martineau, G. D. Watt and R. K. Watt, *J. Inorg. Biochem.*, 2012, **108**, 8–14.

34 H. Q. Huang, Q. M. Lin and Z. B. Lou, *Protein J.*, 2000, **19**, 441–447.
35 S. Lobreaux, S. J. Yewdall, J. F. Briat and P. M. Harrison, *Biochem. J.*, 1992, **288**, 931–939.
36 H. Q. Huang, Z. Q. Xiao, X. Chen, Q. M. Lin, Z. W. Cai and P. Chen, *Biophys. Chem.*, 2004, **111**, 213–222.
37 S. Yun, S. Yang, L. Huang, X. Qi, P. Mu and G. Zhao, *Food Res. Int.*, 2012, **48**, 271–276.
38 L. I. Cheng-Hua, J. Cui, L. I. Ye, J. Zhou, S. U. Xiu-Rong and L. I. Tai-Wu, *Oceanol. Limnol. Sin.*, 2011, **42**, 567–572.
39 L. Chen, J. Zhou, Y. Zhang, S. Chu, W. He, L. Ye and X. Su, *PLoS One*, 2015, **10**, e0119427.
40 T. Wiseman, S. Williston, J. F. Brandts and L. N. Lin, *Anal. Biochem.*, 1989, **179**, 131–137.
41 F. Bouabdallah, P. Arosio, P. Santambrogio, X. Yang, C. Januschandler and N. D. Chasteen, *Biochemistry*, 2002, **41**, 11184–11191.
42 Y. Zhang, A. Shreeram Akilesh and D. E. Wilcox, *Inorg. Chem.*, 2000, **39**, 3057–3064.
43 Y. Zhang and D. E. Wilcox, *JBIC, J. Biol. Inorg. Chem.*, 2002, **7**, 327–337.
44 X. Yang, P. Arosio and N. D. Chasteen, *Biophys. J.*, 2000, **78**, 2049–2059.
45 X. Yang and N. D. Chasteen, *Biophys. J.*, 1996, **71**, 1587–1595.
46 S. Z. Abdullah, P. R. Bérubé and D. J. Horne, *J. Membr. Sci.*, 2014, **463**, 113–125.
47 M. Ananyev, A. Gavrilyuk, S. Mitri, A. Demin, V. Malkov and P. Tsiakaras, *Electrochim. Acta*, 2014, **125**, 371–379.
48 U. Trdan and J. Grum, *Corros. Sci.*, 2014, **82**, 328–338.
49 L. Zhang, J. Liu, H. Xiao, D. Liu, Y. Qin, H. Wu, H. Li, D. Na and W. Hou, *Chem. Eng. J.*, 2014, **250**, 1–5.
50 H. Q. Huang, F. Z. Zhang, L. S. Xu, Q. M. Lin, J. W. Huang and D. Zeng, *Bioelectrochem. Bioenerg.*, 1998, **44**, 301–307.
51 J. Y. Zhu, H. Q. Huang, X. D. Bao, Q. M. Lin and Z. Cai, *Aquat. Toxicol.*, 2006, **78**, 127–135.
52 A. Gonzalvez, S. Armenta and M. D. L. Guardia, *TrAC, Trends Anal. Chem.*, 2009, **28**, 1295–1311.
53 V. S. Selih, M. Sala and V. Drgan, *Food Chem.*, 2014, **153**, 414–423.
54 Y. H. Wei, J. Y. Zhang, D. W. Zhang, L. G. Luo and T. H. Tu, *Food Chem.*, 2014, **159**, 507.
55 A. Bibak, S. Stürup, V. Haahr, A. Pernille Gundersen and V. Gundersen, *J. Agric. Food Chem.*, 1999, **47**, 2678–2684.
56 N. Khan, Y. C. Ji, E. Y. Nho, N. Jamila, G. Habte, J. H. Hong, I. M. Hwang and K. S. Kim, *Food Chem.*, 2014, **158**, 200–206.
57 Y. K. Kwon, Y. S. Bong, K. S. Lee and G. S. Hwang, *Food Chem.*, 2014, **161**, 168–175.
58 L. Huang, Z. C. Lin, Q. Lin, L. Z. Luo and H. Q. Huang, *Chem. Res. Chin. Univ.*, 2008, **24**, 550–556.
59 H. Q. Huang, H. U. Xiao-Hui, X. P. Fang, T. M. Cao and B. Kong, *Chin. J. Anal. Chem.*, 2009, **37**, 631–636.
60 L. Z. Luo, H. W. Jin, Z. W. Cai and H. Q. Huang, *Chin. J. Anal. Chem.*, 2011, **39**, 155–162.
61 H. Huang, R. K. Watt, R. B. Frankel and G. D. Watt, *Biochemistry*, 1993, **32**, 1681–1687.
62 H. Q. Huang, Q. M. Lin, B. Kong, R. Y. Zeng, Y. H. Qiao, C. H. Chen, F. Z. Zhang and L. S. Xu, *Protein J.*, 1999, **18**, 497–504.
63 B. Kong, H. Q. Huang, Q. M. Lin, W. S. Kim, Z. Cai, T. M. Cao, H. Miao and D. M. Luo, *Protein J.*, 2003, **22**, 61–70.
64 G. Matheis, *Food Chem.*, 1991, **39**, 13–26.
65 R. Xing, X. Wang, C. Zhang, Y. Zhang, Q. Wang, Z. Yang and Z. Guo, *J. Inorg. Biochem.*, 2009, **103**, 1039–1044.
66 H. Subramanian, M. Jaganathan and A. Dhathathreyan, *Nano Hybrids*, 2016, **12**, 33–41.
67 X. Liu and E. C. Theil, *Acc. Chem. Res.*, 2005, **38**, 167–175.
68 B. Maity, S. Abe and T. Ueno, *Nat. Commun.*, 2017, **8**, 14820.
69 C. Pozzi, S. Ciambellotti, C. Bernacchioni, F. D. Pisa, S. Mangani and P. Turano, *Proc. Natl. Acad. Sci. U. S. A.*, 2017, **114**, 2580–2585.
70 C. Sun, Y. Yuan, Z. Xu, T. Ji, Y. Tian, S. Wu, J. Lei, J. Li, N. Gao and G. Nie, *Bioconjugate Chem.*, 2015, **26**, 193–198.
71 F. Bou-Abdallah, P. Arosio, S. Levi, C. Janus-Chandler and N. D. Chasteen, *JBIC, J. Biol. Inorg. Chem.*, 2003, **8**, 489–497.
72 P. Santambrogio, P. Pinto, S. Levi, A. Cozzi, E. Rovida, A. Albertini, P. Artymiuk, P. M. Harrison and P. Arosio, *Biochem. J.*, 1997, **322**, 461–468.
73 V. J. Wade, S. Levi, P. Arosio, A. Treffry, P. M. Harrison and S. Mann, *J. Mol. Biol.*, 1991, **221**, 1443–1452.
74 M. A. Kilic, S. Spiro and G. R. Moore, *Protein Sci.*, 2003, **12**, 1663–1675.